JOURNAL OF AIRCRAFT
Vol. 29, No. 4, July–Aug. 1992

Airdata Calibration Techniques for Measuring Atmospheric Wind Profiles

Edward A. Haering Jr.*
NASA Dryden Flight Research Facility, Edwards, California 93523

The research airdata system of an instrumented F-104 aircraft has been calibrated to measure winds aloft in support of the space shuttle wind measurement investigation at the National Aeronautics and Space Administration Dryden Flight Research Facility. For this investigation, wind measurement accuracies comparable to those obtained from Jimsphere balloons were desired. This required an airdata calibration more accurate than needed for most aircraft research programs. The F-104 aircraft was equipped with a research pitot-static noseboom with integral angle-of-attack and flank angle-of-attack vanes and a ring-laser-gyro inertial reference unit. Tower fly-bys and radar acceleration-decelerations were used to calibrate Mach number and total temperature. Angle of attack and angle of sideslip were calibrated with a trajectory reconstruction technique using a multiple-state linear Kalman filter. The F-104 aircraft and instrumentation configuration, flight test maneuvers, data corrections, calibration techniques, and resulting calibrations and data repeatability are presented. Recommendations for future airdata systems on aircraft used to measure winds aloft are also given.

Introduction

THE most common method of obtaining atmospheric wind profiles involves tracking a rising balloon (Jimsphere or Rawinsonde) which moves with the winds. Balloon methods are adequate for many applications but have some limitations. For example, it is impossible to control a balloon's flight path once launched. In addition, the typical rise rate is approximately 15 ft/s (5 m/s), so approximately an hour is required to obtain an altitude of 60,000 ft (18,000 m). For certain applications, such as the space shuttle program, it is desirable to obtain wind profiles quickly, in approximately 10–15 min.

The preprogrammed launch trajectory for the space shuttle is based partially on an expected wind profile for the time of year. If the winds on the day of launch are significantly different from the expected winds, certain shuttle structural load limits may be exceeded. Currently, winds are measured on the day of launch by a series of Jimsphere balloons. The last balloon for loads assessment is launched 2 h before shuttle launch. After the balloon reaches 60,000 ft (18,000 m), the wind data are used in trajectory simulation and loads prediction programs. A wind persistence factor is added to the calculations to account for wind changes over time and the possibility that the balloon has blown away from the launch path. Studies have shown that these changes increase significantly when delays are longer than 2 h or spatial separations are greater than 12 miles (20 km).[1-3] Depending on the results of the loads predictions, a go-no-go recommendation for launch is made.

A reduction in the uncertainties in the prelaunch wind load assessment caused by temporal and spatial variabilities was desired. The National Aeronautics and Space Administration (NASA) Johnson Space Center requested the NASA Dryden Flight Research Facility to perform a flight experiment to determine the feasibility of using an instrumented high-performance aircraft to measure wind profiles. For this technique to be applicable to the space shuttle program, the following guidelines were suggested: 1) obtaining a profile to 60,000 ft (18,000 m) in 10 min; 2) an aircraft profile area within a 10 miles (16 km) radius circle; and 3) measurement accuracy comparable to the Jimsphere system. Winds are calculated as the vector difference between aircraft inertial velocity, measured by an onboard inertial reference unit (IRU) or ground based radar, and aircraft airspeed, measured by a calibrated airdata system.

The quality of the wind profiles measured by Jimsphere balloons can be shown by the repeatability of separate balloons. Studies show that the root mean square (rms) repeatability of wind profiles from two Jimsphere balloons is approximately 7–10 ft/s (2–3 m/s) if the time separation is less than 1 h or the distance separation is less than 12 miles (20 km).[1-3] This is comparable to 0.007–0.010 in Mach number and 0.2–0.3 deg in flow angles at Mach 2. (Actual aircraft wind measurement repeatability depends on the accuracy of several sensors as well as on the atmospheric variability between wind measurements.) Because of these tight tolerances on Mach number and flow angles, an airdata calibration more accurate than required for most aircraft research programs is necessary.

This paper covers the methods and results of the airdata calibration of an F-104 aircraft used to measure winds aloft in support of the F-104 shuttle wind measurement investigation. Wind profile data were gathered at altitudes from 3,000 to 67,000 ft (900 to 20,400 m), Mach numbers from 0.78 to 2, angles of attack from 0 to 12 deg, and angles of sideslip from −3 to 3 deg. The F-104 aircraft and instrumentation configuration, flight test maneuvers, data corrections, calibration techniques, and resulting calibrations and data repeatabilities for Mach number, total temperature, and flow angles are presented in this report. Recommendations for future airdata systems on aircraft used to measure winds aloft are also given. The wind measurement methods and comparisons to Jimsphere balloons for this experiment are documented in Ref. 4.

Description of Aircraft and Instrumentation

The aircraft used for the wind-measurement flight tests was an instrumented F-104 (Fig. 1). A standard National Advisory

Presented as Paper 90-0230 at the AIAA 28th Aerospace Sciences Meeting, Reno, NV, Jan. 8–11, 1990; received Aug. 2, 1990; revision received June 12, 1991; accepted for publication July 28, 1991. Copyright © 1989 by the American Institute of Aeronautics and Astronautics, Inc. No copyright is asserted in the United States under Title 17, U.S. Code. The U.S. Government has a royalty-free license to exercise all rights under the copyright claimed herein for Governmental purposes. All other rights are reserved by the copyright owner.

*Aerospace Engineer, Aerodynamics Branch (XRA). Member AIAA.

Committee for Aeronautics (NACA) research noseboom (Fig. 2) was used to measure static and total pressures and angles of attack and sideslip.[5] Total pressure and static pressure were each measured with a separate high-resolution, high-accuracy absolute-pressure transducer. Total temperature was measured by a nondeiced, open element sensor. Angle-of-attack and flank angle-of-attack values from the vanes were measured using potentiometers. Traditionally, flank angle of attack, β_F, is referred to as angle of sideslip, β.[5] These two quantities are not exactly the same. Flank angle of attack is the rotation of the freestream velocity vector about the body Z axis, and it is what the lower vane on the noseboom measures (Fig. 2). Angle of sideslip is the rotation of the freestream velocity vector about the stability Z axis.[6] The mathematical relationship between these two angles is given later. These two angles are equal at 0 deg angle of attack, and their difference increases as angle of attack is increased. This paper uses the precise definitions of these two terms as opposed to the popular definitions. Research parameters were digitally encoded using pulse code modulation (PCM) and were both recorded onboard and telemetered to ground-based recorders.

A commercial airline aircraft type ring-laser-gyro inertial reference unit (IRU) was used to give inertial velocity, acceleration, attitude, and angular velocity.[7] An airborne instrumentation computer system (AICS) interfaced the IRU with the PCM system and supplied the IRU with inputs from the airdata system.[8] These inputs are needed to stabilize the IRU integration loop.

Since the IRU was designed for commercial airline aircraft, its parameters, especially normal acceleration, were heavily low-pass-filtered. Because high rate maneuvers were used for the flow angle calibrations, it was decided to use a separate accelerometer set located behind the cockpit. The aircraft also had equipment which allowed trajectory guidance information to be telemetered from the ground and displayed to the pilot.[9]

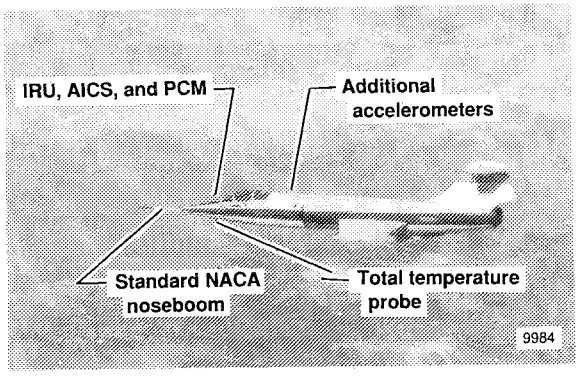

Fig. 1 The F-104 aircraft.

Procedure

Mach Number Calibration

Mach number was calibrated using tower fly-by and radar acceleration-deceleration methods. For the tower fly-by method, shown in Fig. 3, the aircraft is flown at a steady airspeed and altitude near the fly-by tower.[10] The aircraft is sighted from the tower through an eyepiece and grid and the aircraft's true geometric altitude (Z) is determined by geometry. The freestream static pressure at the aircraft's altitude, ($P_{s\infty}$) is calculated using the formula

$$P_{s\infty} = P_{sfb} e^{\left[\frac{Z_{fb} - Z}{RT_{fb}}\right]} \tag{1}$$

where P_{sfb}, T_{fb}, and Z_{fb}, are the static pressure, ambient air temperature, and geometric altitude at the fly-by tower reference altitude, respectively. This formula is the integral form of the hydrostatic equation.[11] The total pressure measured by the noseboom (P_{tot_i}) is assumed to be correct,[12] and the freestream Mach number (M_∞) for subsonic flight is calculated using the expression

$$M_\infty = \sqrt{\frac{2}{\gamma - 1}\left[\left(\frac{P_{\text{tot}_i}}{P_{s\infty}}\right)^{\frac{\gamma-1}{\gamma}} - 1\right]} \tag{2}$$

where γ is the ratio of specific heats for air, 1.4. Indicated Mach number (M_i) is calculated using Eq. (2) with indicated

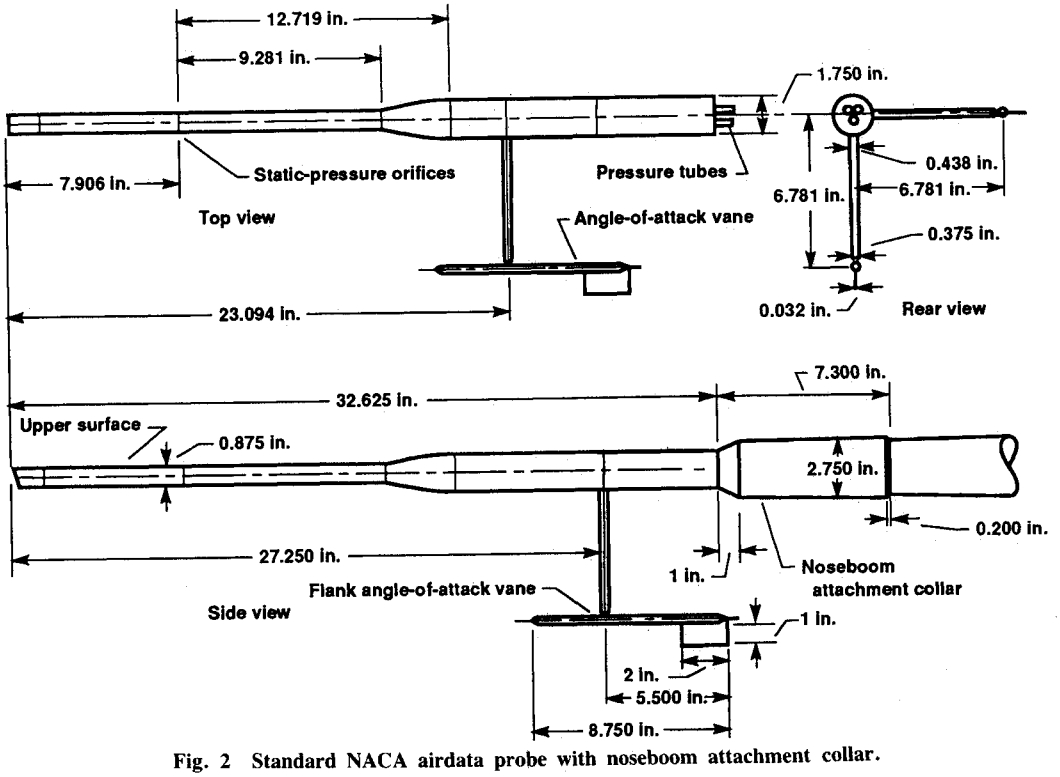

Fig. 2 Standard NACA airdata probe with noseboom attachment collar.

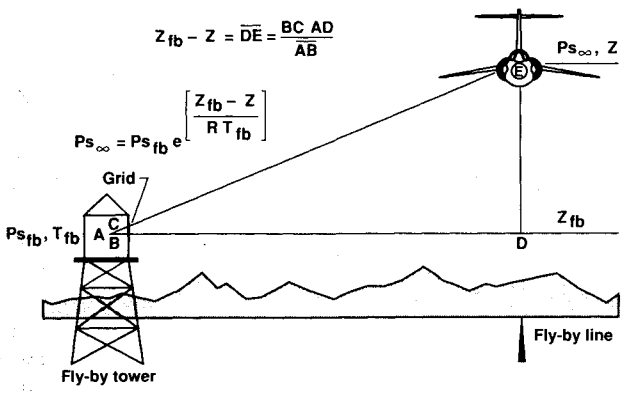

Fig. 3 Tower fly-by position error calibration method.

static pressure (P_{s_i}) substituted for freestream static pressure. Passes by the tower are flown at various subsonic Mach numbers, and the Mach correction

$$\Delta M = M_\infty - M_i \tag{3}$$

is plotted against indicated Mach number to give the Mach calibration. The calibration was assumed to be a function of indicated Mach number only, since high-lift-coefficient flight was not part of the investigation. The tower fly-by technique is the most accurate method, but only subsonic data can be taken, and only a small number of calibration points can be flown on one flight.

In the radar acceleration-deceleration technique (Fig. 4), as in the tower fly-by technique, freestream static pressure is calculated for the aircraft. For a calibration run, the aircraft flies with wings level on a constant heading at a constant geometric altitude. The aircraft's radar altitude is transmitted to the aircraft, and the difference between the desired and actual geometric altitude is displayed in the cockpit to aid the pilot in flying a constant geometric altitude. The aircraft begins the run at a low airspeed and accelerates at approximately 3 kN/s to a peak Mach number. The pilot then begins to decelerate at approximately 3 kN/s back to the original low airspeed. The entire maneuver is executed at radar elevation angles above 10 deg to minimize radar refraction errors and below 80 deg to avoid high radar antennae slew rates.[13] Time coded radar data is processed to give geometric altitude. Weather balloon and atmospheric chart data are analyzed to obtain a table of geometric altitude minus pressure altitude $(Z - hp)_m$ as a function of geometric altitude (Z). The pressure altitude error caused by lateral atmospheric pressure gradient (Δhp_m) with lateral distance and direction from the radar site is also tabulated as a function of geometric altitude. Applying these tables to the time history of the aircraft's radar altitude yields the true pressure altitude of the aircraft, which is then converted into freestream static pressure.[14] As with the tower fly-by method, indicated total pressure is assumed to be true in subsonic flight, and only normal shock losses are assumed in supersonic flight.[12] Equation (2) is then used to calculate freestream Mach number subsonically, (when $P_{tot_i}/P_{s_\infty} < 1.89293$, the value at $M_\infty = 1.0$). The equation

$$M_\infty = \frac{\sqrt{1.42857 - 0.357143Q - 0.0625Q^2 - 0.025Q^3 - 0.012617Q^4 - 0.00715Q^5 - 0.0043458Q^6 - 0.0087725Q^9}}{Q} \tag{4}$$

where

$$Q = 1.839371 \left(\frac{P_{s_\infty}}{P_{tot_i}}\right)$$

is used supersonically, (when $P_{tot_i}/P_{s_\infty} > 1.89293$). This equation is a Taylor series expansion of the Raleigh pitot-static equation.[14] Indicated Mach number is calculated by using Eqs. (2) and (4) with indicated static pressure replacing freestream static pressure. As with the tower fly-by data, Eq. (3) is used to obtain the Mach correction. The result is plotted against indicated Mach number. The radar acceleration-deceleration method is useful because: 1) it allows supersonic Mach calibration; 2) it is independent of the tower fly-by method; 3) the entire Mach calibration can be obtained in a few minutes of flight time; and 4) the maneuvers can be conducted at several altitudes to check for altitude effects on calibration.

Total Temperature Calibration

The ambient air temperature at the aircraft altitude (T_∞) may be calculated from the measured total temperature (T_{tot}), and freestream Mach number by

$$T_\infty = \frac{T_{tot}}{1 + \frac{\gamma - 1}{2} k M_\infty^2} \tag{5}$$

where k is the recovery factor of the total temperature sensor. The value of k is usually a constant parameter and is dependent on the sensor geometry. The recovery factor can be calculated using tower fly-by and radar acceleration-deceleration data. If total temperature is plotted as a function of freestream Mach number squared, the slope is $(\gamma - 1)/2\ T_\infty$, k, and the y-intercept is the freestream temperature. A least-squares curve fit was used to determine these quantities. The value of the recovery factor for the aircraft is taken to be the average from all the maneuvers analyzed.

Flow Angle Corrections

The vanes on the noseboom measure the angles between the local velocity vector and the noseboom axes. Figure 5 shows the steps taken to correct these angles to true angles of attack and sideslip: 1) noseboom misalignment correction, 2) aircraft angular-rate correction, 3) noseboom bending correction, 4) aerodynamic flow angle calibration correction, and 5) transformation of flank angle of attack to angle of sideslip. The first, second, third, and fifth steps are analytical corrections. The fourth is determined through trajectory reconstruction techniques. The fifth step is a geometric transformation.

Noseboom Misalignment Corrections

The first correction to the flow angles (Fig. 5) is for noseboom misalignment. The noseboom on an aircraft may be imperfectly aligned with the aircraft axes. To transform the angles from the noseboom axes system (X_n, Y_n, and Z_n) to the aircraft axes system (X_a, Y_a, and Z_a), the three components of the true airspeed in the noseboom axes system (u_n, v_n, and w_n) must be calculated. The freestream velocity is calculated by

$$V_\infty = M_\infty \sqrt{\gamma R g_0 T_\infty} \tag{6}$$

where R is the ideal gas constant and g_0 is acceleration due to gravity. The three components of airspeed are then evaluated

$$u_n = \frac{V_\infty}{\sqrt{1 + \tan^2(\alpha_i) + \tan^2(\beta_{F_i})}}$$
$$v_n = u_n \tan(\beta_{F_i}) \tag{7}$$
$$w_n = u_n \tan(\alpha_i)$$

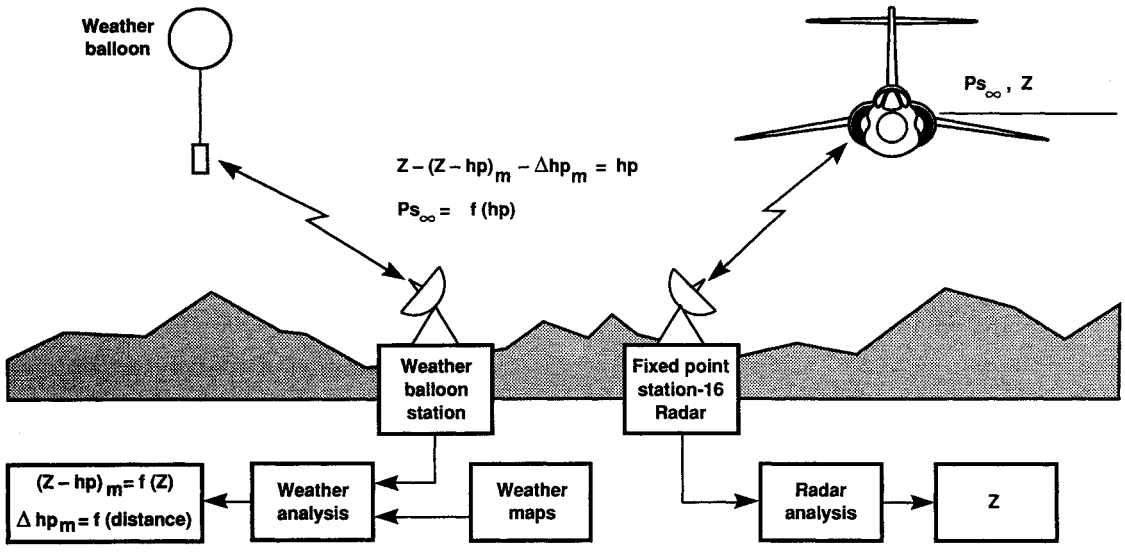

Fig. 4 Radar acceleration-deceleration position error calibration method.

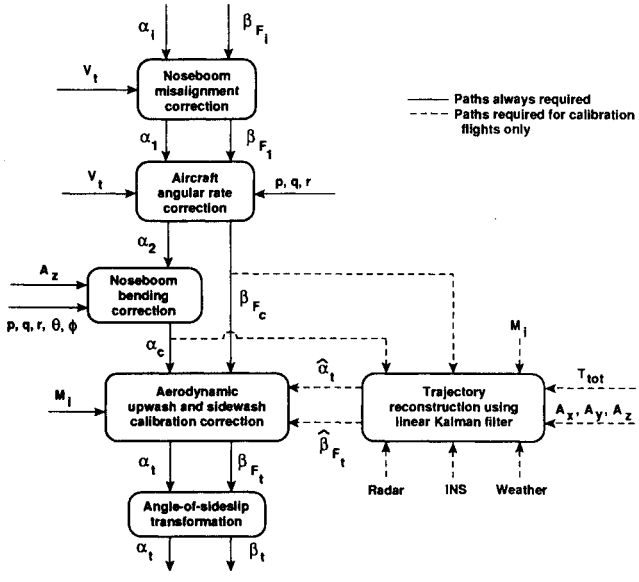

Fig. 5 Flow angle correction steps.

where α_i is the indicated angle of attack and β_{F_i} is the indicated flank angle of attack. The angular offset of the noseboom in roll (ϕ'), pitch (θ'), and yaw(ψ') is measured from the aircraft axes to the noseboom axes. A Euler rotation through these angles transforms the noseboom axes (u_n, v_n, and w_n) components into the aircraft axes (u_a, v_a, and w_a)

$$\begin{bmatrix} u_a \\ v_a \\ w_a \end{bmatrix} = \Gamma \begin{bmatrix} u_n \\ v_n \\ w_n \end{bmatrix} \tag{8}$$

where

$$\Gamma = \begin{bmatrix} \cos(\psi') & -\sin(\psi') & 0 \\ \sin(\psi') & \cos(\psi') & 0 \\ 0 & 0 & 1 \end{bmatrix}$$

$$\begin{bmatrix} \cos(\theta') & 0 & \sin(\theta') \\ 0 & 1 & 0 \\ -\sin(\theta') & 0 & \cos(\theta') \end{bmatrix} \begin{bmatrix} 1 & 0 & 0 \\ 0 & \cos(\phi') & -\sin(\phi') \\ 0 & \sin(\phi') & \cos(\phi') \end{bmatrix}$$

The indicated angle of attack and flank angle of attack can be expressed in the aircraft axes system by

$$\begin{aligned} \alpha_1 &= \tan^{-1}(w_a/u_a) \\ \beta_{F_1} &= \tan^{-1}(v_a/u_a) \end{aligned} \tag{9}$$

The axes system transformation was necessary because of the high accuracy of the angle-of-attack and sideslip measurements needed to accurately measure winds. At an angle of attack of 20 deg and an angle of sideslip of 5 deg, using the pitch and yaw misalignments given in Check 1 of Table 1 as biases to angle of attack and flank angle of attack respectively would result in a 0.5-deg error in flow angle.

The noseboom is fastened to the aircraft radome, which is removed periodically for maintenance. After removing and reinstalling the radome, the boom misalignment measurement is repeated. The values for the offset angles for two flight periods are given in Table 1. These quantities vary by a significant amount.

Aircraft Angular-Rate Corrections

The second correction to the flow angles (Fig. 5) is for angular rates of the aircraft. As the aircraft rolls, pitches, and yaws, the motion of the noseboom about the center of gravity (c.g.) induces additional airspeed components, deflecting the flow vanes. For angle of attack, the pitching and rolling effects of the aircraft were accounted for by

$$\alpha_2 = \alpha_1 + \sin^{-1}[(q\bar{x}_\alpha - p\bar{y}_\alpha)\cos(\alpha_1)/V_\infty] \tag{10}$$

where p, q, and r are the aircraft roll, pitch, and yaw rates, respectively, and $\bar{x}_\alpha$ and $\bar{y}_\alpha$ are the longitudinal and lateral distances from the aircraft (c.g.) to the angle-of-attack vane. These distances are tabulated in Table 2. For flank angle of attack, rolling and yawing effects are accounted for by

$$\beta_{F_c} = \beta_{F_1} + \sin^{-1}[(p\bar{z}_\beta - r\bar{x}_\beta)\cos(\beta_{F_1})/V_\infty] \tag{11}$$

where $\bar{z}_\beta$ and $\bar{x}_\beta$ are the normal and longitudinal distances from the aircraft c.g. to the flank angle-of-attack vane. These are also given in Table 2. Equations (10) and (11) are not limited by small angle approximations and are applicable to high angle-of-attack and high angle-of-sideslip calculations. Any phase lag in the angular-rate corrections due to high angular accelerations has been neglected.

Table 1 Noseboom misalignment

Flight period	ϕ', deg	θ', deg	ψ', deg
Check 1	−1.33	−0.40	0.53
Check 2	−1.25	−0.23	0.27

Table 2 Sensor transformation distances

Parameter	Distance from c.g., ft	Distance from noseboom to accelerometer, ft
$\bar{x}_\alpha$	35.12	
$\bar{y}_\alpha$	−0.57	
$\bar{x}_\beta$	34.77	
$\bar{z}_\beta$	1.09	
$\bar{\bar{x}}_z$		−20.15
$\bar{\bar{y}}_z$		0.2552
$\bar{\bar{z}}_z$		−1.130

Noseboom Bending Correction

The third flow angle correction (Fig. 5) is for noseboom bending. During elevated-g maneuvering, the noseboom deflects under the increased load. The noseboom deflection in pitch caused by elevated g (θ'_g) was measured experimentally for this aircraft as −0.064 deg/g. No correction is made for noseboom bending in the yaw plane, since the aircraft is not significantly loaded in that plane. Also any phase lag in the bending correction due to high angular accelerations has been neglected.

The aircraft's accelerometer package is located behind the cockpit in the electrical bay, so acceleration data must be translated to the noseboom before the noseboom deflection can be calculated. Table 2 presents the distances $\bar{\bar{x}}_z$, $\bar{\bar{y}}_z$, and $\bar{\bar{z}}_z$, from the noseboom to the vertical accelerometer (A_z). The normal acceleration at the noseboom (A_b) is

$$A_b = -A_z + \frac{(pr - \dot{q})\bar{\bar{x}}_z + (qr + \dot{p})\bar{\bar{y}}_z - (p^2 + q^2)\bar{\bar{z}}_z}{g_0} \tag{12}$$

Note that for positive g, A_b is positive and A_z is negative. The roll, pitch, and yaw accelerations ($\dot{p}$, $\dot{q}$, and $\dot{r}$) were numerically differentiated from p, q, and r using a five point weighted least-squares sliding window.[15]

Angle of attack corrected for noseboom bending is

$$\alpha_c = \alpha_2 - \theta'_g(A_b - \cos(\theta)\cos(\phi)) \tag{13}$$

where the term involving the cosines subtracts the normal acceleration caused by gravity.

Aerodynamic Flow Angle Calibrations Corrections

The fourth correction to the flow angles (Fig. 5) is for aerodynamic effects that the aircraft and the noseboom induce on the local velocity vector. These effects have been calibrated through flight test data using a trajectory reconstruction algorithm. The corrections for angle of attack will be called upwash, and for flank angle of attack the corrections will be called sidewash.

For subsonic flight, upwash was identified using the following flight test technique. Aided by the uplink, the pilot held the aircraft at a constant altitude, Mach number, and power setting for several seconds, then swept through a range of angle of attack, followed by several seconds of stabilized data. Sidewash was calibrated in a similar fashion with sweeps in flank angle of attack. These maneuvers were conducted at true Mach numbers ranging from 0.78 to 0.92.

Since no flow disturbances from the aircraft can propagate forward to the flow vanes in supersonic flow, upwash and sidewash will not be a function of angle of attack or flank angle of attack. Shock waves on the noseboom affect the indicated flow angles, however, so upwash and sidewash are identified as a function of indicated Mach number, using the radar acceleration-deceleration maneuver described earlier.

The true angle of attack and flank angle of attack are calculated by a trajectory reconstruction algorithm with a multiple-state linear Kalman filter (LKF).[16] The LKF blends data from the aircraft's accelerometers, IRU, airdata system, radar tracking, and weather analysis to give the minimum variance estimate of the aircraft's trajectory. The observations and the dynamics equations are selectively weighted using a matrix determined by physical intuition about the system. The LKF algorithm consists of a prediction and correction step. The prediction step extrapolates the measured data to the next time point using the dynamics equations. The correction step adjusts the extrapolated state using measured data at that next time point to give the minimum variance estimate.[16]

The components of the inertial velocity and winds aloft, calculated by the LKF (denoted by $\hat{}$), were added in vector form to give estimates of true angle of attack and flank angle of attack for each time point in the calibration maneuver, that is, at each data frame. True angle of attack and true flank angle of attack are determined from the LKF reference states as

$$\alpha_t = \tan^{-1}\left[\frac{\hat{w}}{\hat{u}}\right] \tag{14}$$

$$\beta_{F_t} = \tan^{-1}\left[\frac{\hat{v}}{\hat{u}}\right] \tag{15}$$

where

$$\begin{bmatrix} u \\ v \\ w \end{bmatrix} = \Gamma^T \left\{ \begin{bmatrix} V_N \\ V_E \\ V_D \end{bmatrix} - \begin{bmatrix} W_N \\ W_E \\ W_D \end{bmatrix} \right\}$$

$$\Gamma^T = \begin{bmatrix} 1 & 0 & 0 \\ 0 & \cos(\phi) & \sin(\phi) \\ 0 & -\sin(\phi) & \cos(\phi) \end{bmatrix} \tag{16}$$

$$\begin{bmatrix} \cos(\theta) & 0 & -\sin(\theta) \\ 0 & 1 & 0 \\ \sin(\theta) & 0 & \cos(\theta) \end{bmatrix} \begin{bmatrix} \cos(\psi) & \sin(\psi) & 0 \\ -\sin(\psi) & \cos(\psi) & 0 \\ 0 & 0 & 1 \end{bmatrix}$$

V_n, V_E, V_D are the inertial north, east, and down velocity components, and W_N, W_E, W_D are the north, east, and down wind components. There are several things to note in these equations. First, true flank angle of attack is used since it is independent of angle of attack and more directly comparable to corrected flank angle of attack than true angle of sideslip is. Second, the vertical component of the wind measurement is set to zero since it is difficult to measure using weather balloons. Lastly, Γ^T is used to transform the velocity components from earth axes to aircraft body axes.

The errors in angle of attack and flank angle of attack are

$$\Delta\alpha = \alpha_c - \alpha_t \tag{17}$$

$$\Delta\beta_F = \beta_{F_c} - \beta_{F_t} \tag{18}$$

These errors are plotted as functions of corrected angle of attack, corrected flank angle of attack, and indicated Mach number in order to identify systematic trends that can be used for a calibration. Figure 6 shows a typical subsonic angle-of-attack calibration maneuver at a freestream Mach number of 0.92. Once identified, a line is fit to the data using least-squares regression. The slope of the error in angle of attack as a function of corrected angle of attack curve ($\delta\Delta\alpha/\delta\alpha_c$) is defined as the upwash factor, and the slope of the error in flank angle of attack as a function of corrected flank angle of

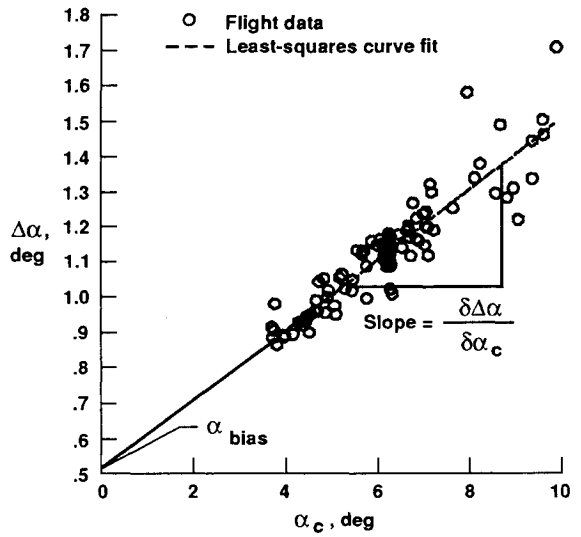

Fig. 6 Typical subsonic angle-of-attack calibration maneuver at $M_\infty = 0.92$.

attack curve ($\delta\Delta\beta_F/\delta\beta_{F_c}$) is the sidewash factor. The y-intercepts of the curves are the angle-of-attack and flank angle-of-attack biases (α_{bias} and $\beta_{F\text{bias}}$). The upwash and sidewash factors are a function of indicated Mach number as is the angle-of-attack bias.

No trend of flank angle-of-attack bias with indicated Mach number was found in this calibration effort for this wind measurement investigation. The high sensitivity of flank angle of attack to small errors in the wind estimate makes this task impossible without many more data flights to get a statistically significant set of data points to assure that the resulting mean error is near zero. This is a limitation of the method, since it relies on an accurate measurement of the winds by weather balloons. On flights when there is a relatively large spatial and temporal difference between the aircraft and balloon, wind variability degrades the quality of the horizontal wind profile. This is not a problem for the angle-of-attack bias as zero vertical winds are assumed, which except for severe atmospheric phenomena, is a good assumption.

Subsonically, the true angle of attack and true flank angle of attack are calculated by

$$\alpha_t = \alpha_c - \left[\frac{\delta\Delta\alpha}{\delta\alpha_c}\alpha_c + \alpha_{\text{bias}}\right] \tag{19}$$

$$\beta_{F_t} = \beta_{F_c} - \left[\frac{\delta\Delta\beta_F}{\delta\beta_{F_c}}\beta_{F_c} + \beta_{F\text{bias}}\right] \tag{20}$$

for $M_i < 1.0$.

As noted previously, in supersonic flight flow angle errors are a function of Mach number only. The trend with Mach number is continuous and repeatable outside of the transonic region, where local shock waves interfere with the flow vanes.[17] True angle of attack and true flank angle of attack for supersonic flight are

$$\alpha_t = \alpha_c - \Delta\alpha \tag{21}$$

$$\beta_{F_t} = \beta_{F_c} - \Delta\beta_f \tag{22}$$

for $M_i > 1.0$.

The calibration coefficients can be used as long as the external configuration of the aircraft is not significantly altered and the sensors have not degraded. It is important to have preflight inspections of the noseboom, total temperature sensor, IRU, and supporting electronics to assure quality data will be gathered.

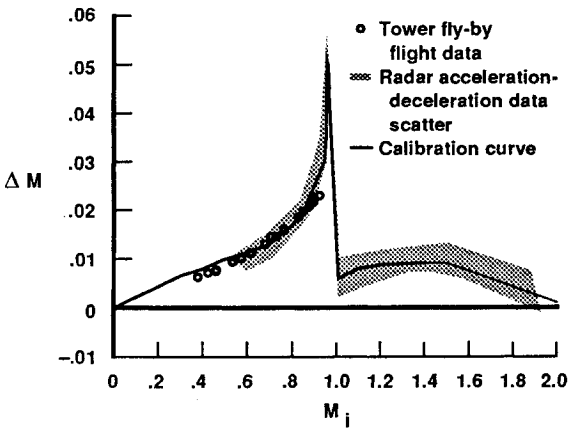

Fig. 7 Mach number position error calibration.

Table 3 Total temperature recovery factor calibrations

Maneuver	Recovery factor, k
1	0.9897
2	0.9953
3	0.9913
4	0.9766
5	0.9786
Average k	0.986

Transformation of Flank Angle of Attack to Angle of Sideslip

The fifth and last correction to the flow angles (Fig. 5) is the transformation of flank angle of attack to angle of sideslip, given by

$$\beta_t = \tan^{-1}[\tan(\beta_{F_t})\cos(\alpha_t)] \tag{23}$$

since

$$\beta_t = \sin^{-1}\left[\frac{v}{V_\infty}\right] \tag{24}$$

As noted previously, angle of sideslip and flank angle of attack are equal at an angle of attack of 0 deg.

Results and Discussions

Mach Number Calibration

To calibrate Mach number for this aircraft, 22 tower fly-by points and 11 radar acceleration-deceleration maneuvers were obtained and analyzed. Figure 7 shows the Mach number calibration correction as a function of indicated Mach number for all the calibration maneuvers. As Fig. 7 shows, the scatter is approximately ± 0.003 in the subsonic data, and approximately ± 0.005 in the supersonic data. A curve faired through the data was used as the Mach number calibration, shown in Fig. 7 as a solid line.

Total Temperature Calibration

Total temperature was calibrated by extracting the recovery factor from tower fly-by and radar acceleration-deceleration data. Table 3 shows the individual recovery factors with magnitudes varying from 0.977 to 0.995, with an average of 0.986. Some of the ± 0.009 scatter is caused by variations in ambient air temperature during the calibration maneuvers, especially for the tower fly-by maneuvers which were conducted over more than an hour of flight time. Wind-tunnel data for this type of temperature sensor yields recovery factors between 0.992 and 0.999.[18]

Flow Angle Calibrations

The flow angles for this aircraft were corrected using the five steps shown in Fig. 5. One of these steps was correcting the flow angles for aerodynamic upwash and sidewash.

Subsonic Upwash Calibration

Figure 8 shows the subsonic upwash factor as a function of indicated Mach number. The increase of the upwash factor with increasing Mach number is thought to be caused by a compression effect on the angle-of-attack vane, caused by the proximity to the flank angle-of-attack vane support shaft. Dual flank angle-of-attack vanes, one opposite the original vane, would make the compression field symmetrical about the X_n–Y_n plane, and negate the change in upwash factor with indicated Mach number. The dependence of the angle-of-attack bias on indicated Mach number is shown in Fig. 9, along with its calibration fairing. Comparing the fully calibrated subsonic angle of attack with the LKF estimate yields a residual bound of approximately ± 0.2 deg.

Subsonic Sidewash Calibration

The subsonic sidewash factor plotted as a function of indicated Mach number is shown in Fig. 10. The increase in sidewash factor with increasing Mach number above $M_i = 0.84$ is thought to be caused by a compression effect on the flank angle-of-attack vane caused by the noseboom attachment collar located immediately behind the vane (Fig. 2). The flank angle-of-attack bias had too much scatter to calibrate because of its high sensitivity to errors in the meteorological winds estimate. For these calibrations, the flank angle-of-attack bias was assumed to be zero. Comparing the fully calibrated subsonic flank angle of attack with its LKF reference estimate yields a residual whose variations about the mean are bounded by ± 0.15 deg, meaning sidewash factor has been calibrated to within ± 0.15 deg.

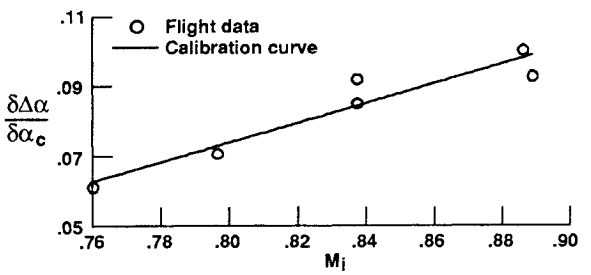

Fig. 8 Subsubsonic upwash factor.

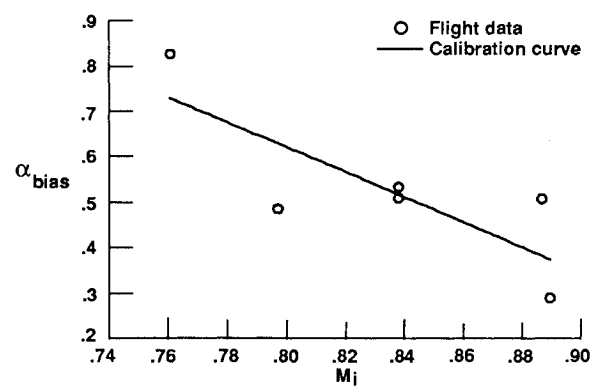

Fig. 9 Subsonic angle-of-attack bias.

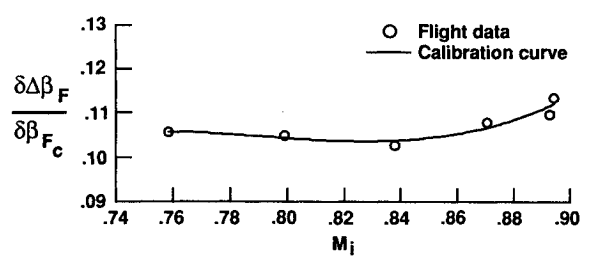

Fig. 10 Subsonic sidewash factor.

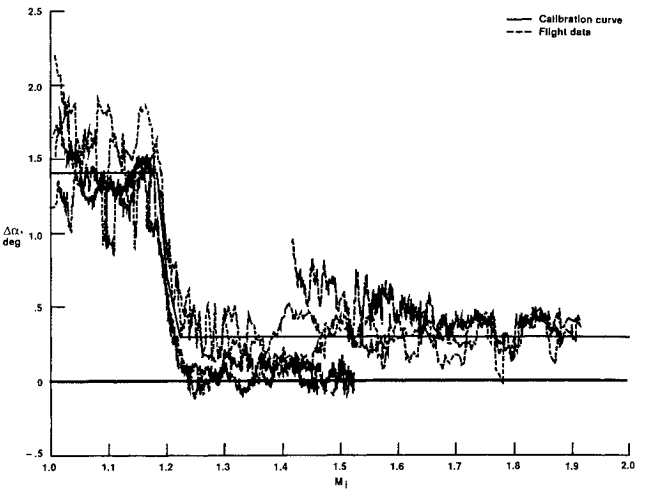

Fig. 11 Supersonic angle-of-attack calibration.

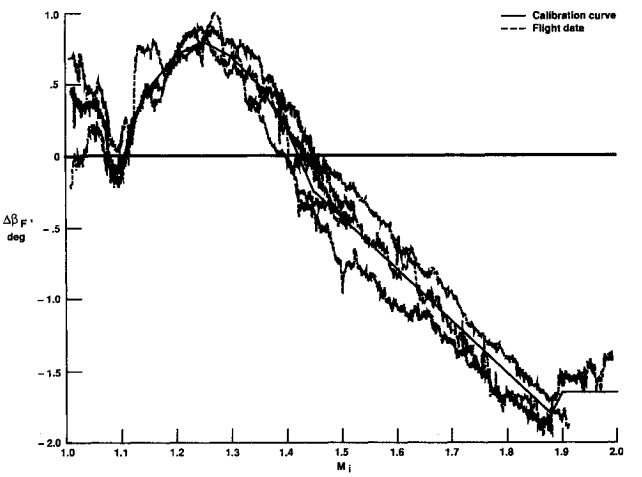

Fig. 12 Supersonic flank-angle-of-attack calibration.

Supersonic Upwash Calibration

Figure 11 shows the supersonic angle-of-attack error as a function of indicated Mach number for several flights with its faired calibration curve. The calibration curve shows a sharp drop in error at $M_i = 1.20$, which is thought to be caused by a local shock wave crossing the angle-of-attack vane. At higher indicated Mach numbers, angle-of-attack error is constant. As Fig. 11 shows, the flight-to-flight scatter in the supersonic angle-of-attack calibration is approximately ± 0.3 deg.

Supersonic Sidewash Calibration

Figure 12 shows the supersonic flank angle-of-attack error as a function of indicated Mach number for several flights along with its faired calibration curve. The decrease in the change in flank angle of attack above $M_i = 1.250$ is thought to be caused by the single angle-of-attack vane. The oblique shock wave off of the angle-of-attack vane and support shaft increases the static pressure on the port side of the noseboom, making the flank angle-of-attack vane read too low. This effect becomes more pronounced as indicated Mach number increases because of the increasing shock strength, as the curve's negative slope shows. Dual angle-of-attack vanes would make the pressure distribution around the noseboom symmetric about the X_n–Z_n plane, negating the Mach effect on

flank angle of attack. As Fig. 12 shows, the flight-to-flight scatter in the supersonic flank angle-of-attack calibration is approximately ±0.25 deg.

Effect of Airdata Calibration on Wind Measurement Quality

Assuming negligible errors in the inertial velocities calculated by the IRU or ground-based radar, the calibration repeatabilities attained should result in measured wind speed repeatabilities of 3 to 10 ft/s (1 to 3 m/s). The airdata repeatabilities, in terms of the calibration error bounds, are similar to the rms repeatability of the radar tracked Jimsphere balloon.[1-3] The wind speed repeatability of 3 ft/s is calculated assuming a Mach number of 0.9, and the 10 ft/s repeatability assumes a Mach number of 2. Since the flow angles are used to resolve the airspeed into wind components, a given error in a flow angle will cause an increasing wind error as aircraft speed increases. For this aircraft, however, high speeds are necessary to obtain high altitudes and to rapidly survey the altitude desired.

Recommendations

Several recommendations from this experiment may be helpful in the design and operation of future airdata systems for aircraft used to measure winds aloft. To minimize the effects of Mach number on the flow angles, dual vanes for both angle of attack and flank angle of attack should be used, making the flow field symmetrical vertically and laterally. Increasing the distance between the sets of angle-of-attack vanes and flank angle-of-attack vanes should reduce the compression effect on the vanes, and eliminating the noseboom attachment collar will eliminate any compression effect on the flank angle-of-attack vanes.

Since an accurate knowledge of the angular offset of the noseboom from the IRU is necessary for a successful calibration these two systems should be rigidly attached to the same structure. The structure should have a location to measure externally roll, pitch, and yaw angles on the ground. This would minimize the effects of maintenance and aircraft bending and torsion in flight on the misalignment angles.

Concluding Remarks

The research airdata system of an F-104 aircraft has been calibrated to measure winds aloft. The wind measurement accuracy desired for this investigation required an airdata calibration more accurate than for most aircraft research programs. Mach number was calibrated using the tower fly-by and radar acceleration-deceleration techniques, with a flight-to-flight calibration repeatability of ±0.003 subsonically and ±0.005 supersonically. Total temperature was calibrated and found to have a recovery factor of 0.986 with a ±0.009 scatter in the data.

Flow angles were corrected for noseboom misalignment, time delays, aircraft angular rates, and noseboom bending, then calibrated using trajectory reconstruction using a multiple state linear Kalman filter (LKF). Noseboom misalignment was corrected by a Euler rotation through its offset angles. The flow angles were corrected for aircraft rates without using small angle approximations.

The trajectory reconstruction calibration method using the multiple-state LKF allows several different data sources to be blended, minimizing systematic errors in the data and yielding highly accurate trajectory information. The flight-to-flight calibration repeatability of angle of attack is ±0.2 deg subsonically and ±0.3 deg supersonically, and the flight-to-flight calibration repeatability of flank angle of attack is ±0.15 deg subsonically and ±0.25 deg supersonically. These calibration repeatabilities are considered to be near the attainable accuracy limit with the configuration used. The subsonic flank angle-of-attack bias data had too much scatter to calibrate, probably because of the high sensitivity of the true flank angle-of-attack calculation to small errors in the meteorological wind estimate.

Assuming negligible errors in the inertial velocities calculated by the inertial reference unit or ground-based radar, the airdata calibration repeatabilities attained should result in measured wind speed repeatabilities of 3–10 ft/s (1–3 m/s), approximately the same repeatability as the radar tracked Jimsphere balloon.

Several recommendations from this investigation will be useful in the design and operation of future airdata systems for aircraft used to measure winds aloft. These include using a noseboom with dual angle-of-attack and flank angle-of-attack vanes to reduce the sensitivity of upwash and sidewash on Mach number. The noseboom and inertial reference unit should be rigidly attached to the same structure to minimize geometric alignment variability.

References

[1]Hill, C. K., "Analysis of Jimsphere Pairs for Use in Assessing Space Vehicle Ascent Capability," NASA TP-2573, 1986.

[2]Adelfang, S. I., "Study of Wind Change for the Development of Loads Reduction Techniques for the Space Shuttle," NASA CR-4045, 1987.

[3]Wilfong, T. L., and Boyd, B. F., "Winds Aloft to Support Space and Missile Launches," *Proceedings of the Third International Conference on the Aviation Weather System*, Anaheim, CA, Jan. 3–Feb. 3, 1989, pp. 102–107.

[4]Bjarke, L. J., and Ehernberger, L. J., "An In-Flight Technique for Wind Measurement in Support of the Space Shuttle Program," NASA TM-4154, 1989.

[5]Richardson, N. R., and Pearson, A. O., "Wind-Tunnel Calibrations of a Combined Pitot-Static Tube, Vane-Type Flow-Direction Transmitter, and Stagnation-Temperature Element at Mach Numbers from 0.60 to 2.87," NASA TN D-122, 1959.

[6]Maine, R. E., and Iliff, K. W., "Application of Parameter Estimation to Aircraft Stability and Control, The Output-Error Approach," NASA RP-1168, 1986.

[7]Litton Aero Products, *LTN-90 Inertial Reference Unit Component Maintenance Manual*, 34-47-01, Revision 8, Moorpark, CA, June, 1986.

[8]Bever, G. A., "The Development of an Airborne Instrumentation Computer System for Flight Test," NASA TM-86036, 1984.

[9]Meyer, R. R., Jr., and Schneider, Cdr. E. T., "Real-Time Pilot Guidance System For Improved Flight Test Maneuvers," AIAA Paper 83-2747, Nov., 1983.

[10]De Anda, A. G., "Air Force Flight Test Center Standard Airspeed Calibration Procedures," AFFTC-TIH-81-5, June, 1981.

[11]National Oceanic and Atmospheric Administration, National Aeronautics and Space Administration, United States Air Force, *United States Standard Atmosphere*, 1976.

[12]Gracey, W., "Measurement of Aircraft Speed and Altitude," NASA RP-1046, Hampton, VA, May, 1980.

[13]James, R., and Brownlow, J. D., "Mathematical Analysis Study for Radar Data Processing and Enhancement Part II: Modeling of Propagation Path Error," NASA CR-166616, 1985.

[14]Johnson, J. B., Larson, T. J., and Ficke, J. M., "Digital Program for Calculating Static Pressure Position Error," NASA TM-86726, 1987.

[15]Carnahan, B., Luther, H. A., and Wilkes, J. O., *Applied Numerical Methods*, Wiley, New York, 1969.

[16]Whitmore, S. A., Larson, T. J., and Ehernberger, L. J., "Air Data Position-Error Calibration Using State Reconstruction Techniques," NASA TM-86029, 1984.

[17]Sakamoto, G. M., "Aerodynamic Characteristics of a Vane Flow Angularity Sensor System Capable of Measuring Flightpath Accelerations For the Mach Number Range from 0.40 to 2.54," NASA TN D-8242, 1976.

[18]Stickney, T. M., Shedlov, M. W., Thompson, D. I., and Yakos, F. T., *Rosemount Total Temperature Sensors*, Technical Rept. 5755, Revision A, Rosemount, Inc., Minneapolis, MN, 1981.